

# PERMANENT MAGNET ECRIS FOR THE KEK DIGITAL ACCELERATOR\*

Leo Kwee Wah<sup>1#</sup>, K.Okazaki<sup>2</sup>, T.Arai<sup>3</sup>, T.Adachi<sup>1,3</sup>, K.Takayama<sup>1,3,4</sup>, K. Koyama<sup>3</sup>, and M.Wake<sup>1,3</sup>

<sup>1</sup>The Graduate University for Advanced Studies, KEK, Tsukuba, Ibaraki, Japan

<sup>2</sup>Nippon Advanced Technology Co. Ltd. (NAT), Tokaimura, Ibaraki, Japan

<sup>3</sup>High Energy Accelerator Research Organization (KEK), Tsukuba, Ibaraki, Japan

<sup>4</sup>Tokyo Institute of Technology, Nagatsuda, Kanagawa, Japan

## Abstract

The KEK-Digital Accelerator (DA) is an induction synchrotron renovated from the KEK 500 MeV booster synchrotron [1]. Its concept was demonstrated in 2006 using the 12 GeV proton synchrotron [2,3], where a proton bunch was accelerated with pulse voltages generated by a transformer instead of RF cavity. In the KEK-DA, O, Ne, and Ar ions from the ECRIS embedded in the 200 kV high-voltage terminal (HVT) are directly injected into the ring through the low energy beam transport line. The permanent magnet ECRIS, in which a plasma is fired by x-band microwave pulses of 3 msec at 10 Hz, has been assembled at KEK. Its operational performance such as charge-state spectrum, emittance and current have been tested since the last year. Beam dynamics through the test bench is discussed as well as operational characteristics of the ECRIS.

## INTRODUCTION

The KEK-DA is a recycling of the KEK 500 MeV PS-Booster, which was shut down in March, 2006, and is being renovated as the first DA.

The operational schematic of the ion source and LEBT to the KEK-DA is shown in Fig.1 [1,2]. An ion beam is directly injected into the KEK-DA from the ion source without a gigantic injector. In order to mitigate space-charge effects during injection, the ion beam is accelerated through a high voltage acceleration column of 185 kV.

A permanent magnet ECRIS is a unique solution when an ion source is mounted in a high voltage terminal, because it does not require a large amount of electric power and its size is small and its weight is less than 50 kg. Since 2008 a pulse-mode x-band ECRIS has been developed.

An Ar beam including Ar<sup>1+</sup>~Ar<sup>8+</sup> is extracted through the extraction electrode of 14-15 kV and focused in the downstream Einzel lens system and guided into the acceleration column with inner focusing electrodes and enters into the separation magnet to be selected a desired charge state (*Z*) ion beam. Through the quadrupole focusing channel, an Ar<sup>8+</sup> beam pulse of 3-5 msec long is guided and chopped by an Einzel lens or electrostatic chopper placed at the downstream.

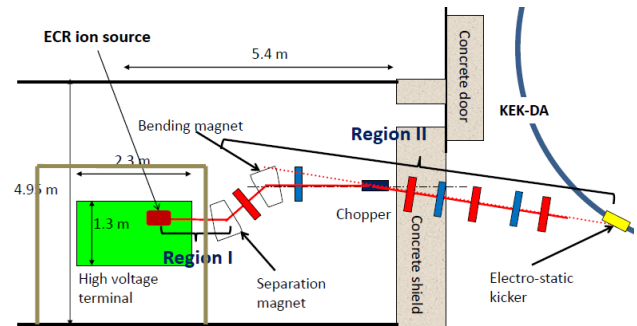


Figure 1: High voltage ion source and LEBT

## ECRIS

The all-permanent magnet ECRIS has been built and tested over the last two years. Presently obtained results are discussed here. In addition remained issues are addressed.

### Mechanical Design

The mechanical design of this ECRIS is shown in Fig. 2. It shows the complete assembly including two permanent ring magnets, hexapole magnet, return yolk, the microwave horn antenna and the extraction system with a screen to protect metal ions from spattering on the surface of the insulating ceramic pipe. The position of the antenna horn aperture can be optimized for matching. A plasma chamber with water cooling channels has been originally designed assuming a CW operation. As a result, the aperture size of 4cm in diameter is rather big compared with a similar x-band permanent ECRIS such as Nanogan [4].

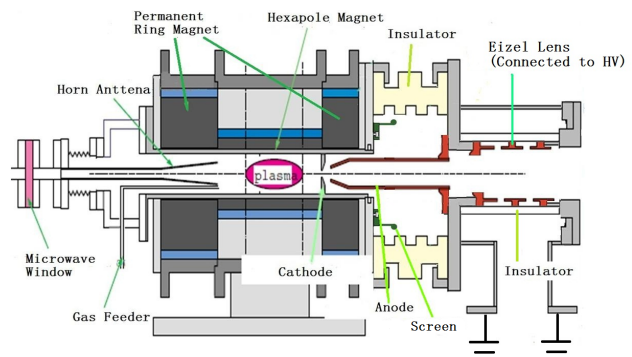


Figure 2: Schematic overview of the X-band ECR for The KEK-DA

\*Supported by Grant-In-Aid for Scientific Research (S) (KAKENHI No. 20224005)

#leokw@post.kek.jp

### Magnetic System

It is well-known that the high axial mirror ratio and a strong radial field inside the plasma chamber are important [5]. For our present ECRIS, the first peak flux density is ( $B_{peak1}$ ) 7 kG, the second peak flux density ( $B_{peak2}$ ) is 5.6 kG and the radial flux density ( $B_r$ ) on the inner surface of the plasma chamber ( $r=20$  mm) is 5 kG. The resonance flux density ( $B_{ECR}$ ) is 3.3 kG for the frequency of 9.35 GHz. The empirical rule [5] tells us  $B_r \sim 2 B_{ECR}$  is desired. The actual field strength is a bit lower than this condition.

### Microwave Heating

9.35 GHz microwaves are provided from a TWT with a maximum power of 700 W. In the present ECRIS, the microwave power in  $TE_{01}$  mode is uniformly irradiated in the plasma chamber from the rectangular horn antenna. Since the KEK-DA is operated at 10 Hz, the injection of ion beams at the same repetition rate is expected. An ion pulse is generated in a pulse mode, where the 5 msec long microwave pulse are fired at 10 Hz by controlling a seed pulse length of the TWT.

### Extraction System

The geometrical shape of the anode hole biased at 14 - 15 kV and the grounded extraction electrode have been optimized by IGUN simulations. In the early stage, spattering of metal ions on the insulating ceramic pipe wall was serious to result in high voltage breakdown. The screen seen in Fig. 2 was quite effective to keep a clean surface from the direct spattering.

### Test Bench

In order to investigate operational performances of our ECRIS including beam parameters and beam stability, a test bench have been constructed. It is divided into two portions: upper stream and downstream. The upper stream consists of a diagnostic device (Faraday Cup) just placed after the Einzel lens measured a total ion current. The beam is focused by a electrostatic quadrupole doublet (D)(F) and guided through the analyzer magnet to downstream. The downstream also consists of another doublet (F)(D) and to the diagnostic devices (Faraday cup and beam profile monitor) which are placed at the end point of the test bench as shown in Fig. 3.

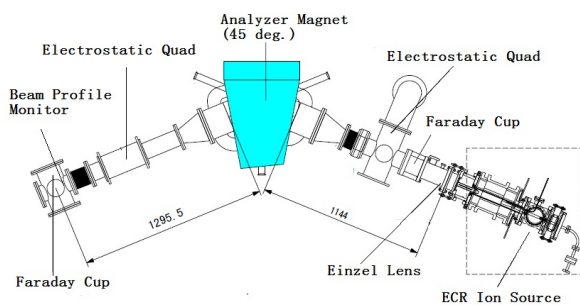


Figure 3: Schematic overview of test bench

### Measurement Results

Charge-state spectrum of the extracted Oxygen, Neon and Argon beam were obtained by monitoring a beam current in the downstream Faraday cup. Figs. 4 and 6 show the pulse shapes for individual charge states at the gas flow rate of 0.05 SCCM for Argon and Neon.

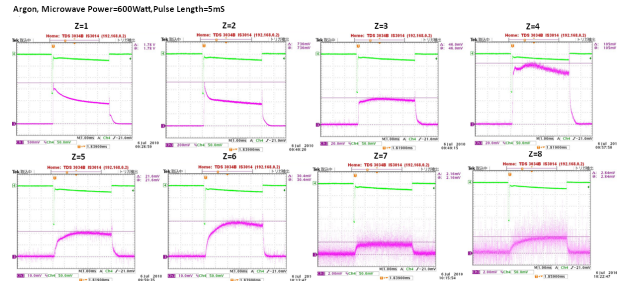


Figure 4: Waveform of ion current. Power/pulse length: 600W/5msec, upper green trace is the reflection signal of microwaves (Argon)

Absolute ion intensities have been obtained as a function of the microwave power. The results are shown in Fig. 5 and 7.

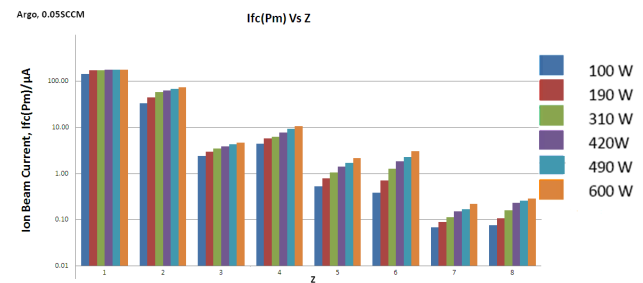


Figure 5: Ion current of an individual charge state for various microwave power (Argon)

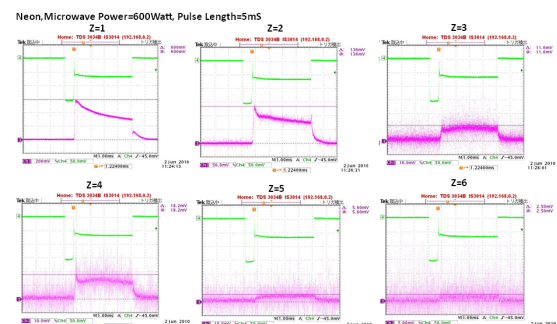


Figure 6: Waveform of ion current. Power/pulse length: 600W/5msec, upper green trace is the reflection signal of microwaves (Neon)

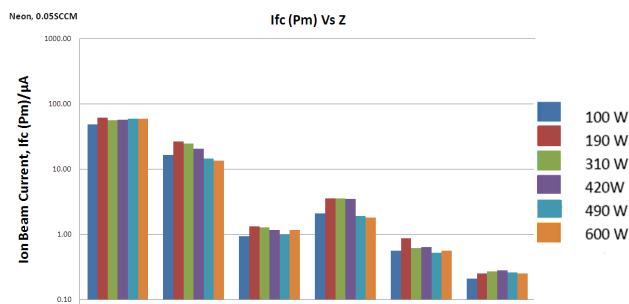


Figure 7: Ion current of an individual charge state for various microwave power (Neon)

### Discussions

Achieved highest charge states for Oxygen, Neon and Argon were 6, 6 and 8, respectively. This fact can be explained by their ionization energy. According to reference [6], the ionization energy ( $\Delta E$ ) of  $\text{Ar}^{7+ \rightarrow 8+}$  is 143.5 eV,  $\text{Ar}^{8+ \rightarrow 9+}$  is 422.4 eV and  $\text{Ne}^{5+ \rightarrow 6+}$  is 157.9 eV,  $\text{Ne}^{6+ \rightarrow 7+}$  is 207.3 eV and  $\text{O}^{5+ \rightarrow 6+}$  is 138.1 eV,  $\text{O}^{6+ \rightarrow 7+}$  is 739.3eV. To obtain higher charge state ions, the electron energy must be sufficiently higher than the required ionization energy for a desired charge state. The achieved charge state of three species of ion suggested the density of high energy electron might be insufficient for ionization to the higher charge state. It is known that the electron confinement time in ECRIS increase as the mirror ratio of the magnetic field increases. This is crucial to obtain highly charged ions. Meanwhile, the so-called magnetic field scaling laws suggest that  $B_{\text{peak1}}/B_{\text{ECR}} \sim 4$  and  $B_r/B_{\text{ECR}} \sim 2$  are desired [7]. Their values in our present ECRIS are 2.1 and 1.5, respectively. The latter seems to be notably small.

### Beam Dynamics

The IGUN simulator has been used to simulate the beam dynamics from the cathode to the anode and from the anode through the Einzel lens as shown in Fig. 8. The beam emittance and phase space plot are generated from the IGUN output.

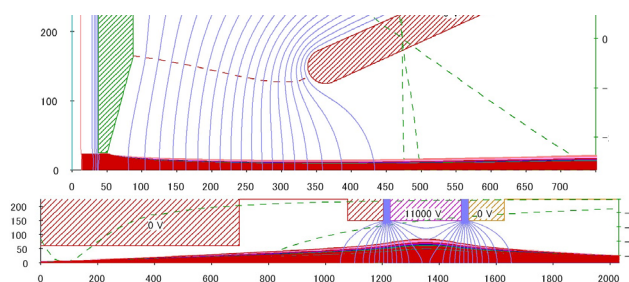


Figure 8: Beam envelope from the cathode to anode and from anode through Einzel Lens (IGUN simulation result)

IGUN simulations based on the Langmuir-Child law [8] give a space-charge limited ion current under an artificial assumption of a relative fractional ratio of charge states. In our calculations, the experimentally obtained fractional ratios were assumed. Consequently,

the estimated space-charge limited current was in good agreement with the experimentally obtained total ion current.

The lattice function at the beginning of the test bench can be evaluated from the IGUN output. It is straightforward to calculate the beam envelope along the beam transport line using this initial value and lattice parameters which are uniquely determined by the voltage of electrostatic Q-lenses. It is interesting to compare the actual beam profile on the X-Y plane with the predicted result. For this purpose, a beam profile measurement was carried out using an emission plate of alumina placed at the end point of the beam line. Basic qualitative features of the observed profile were consistent with the predicted ones.

### SUMMARY

Although our permanent ECRIS can deliver lower charge-state ions with a sufficient intensity, the intensity of higher charge-state ions is not enough. This could be attributed to the low  $B_r$  on the inner surface of the plasma chamber. In addition the region with  $B=B_{\text{ECR}}$  is far from the central region. In order to improve both undesired features, installation of a thinner hexapole magnet into the inner aperture is underway.

### ACKNOWLEDGMENTS

The authors wish to thank Y. Arakida for providing an idea of profile monitoring, Shinozuka and Wakui of Tohoku University for their suggestions on remained issues and A. Takagi for his advice of voltage stabilizing.

### REFERENCES

- [1] K. Takayama, Y. Arakida, T. Iwashita, T. Dixit and K. Torikai, J. of Appl. Phys. 101, 063304 (2007).
- [2] K. Takayama, Y. Arakida, T. Dixit, T. Iwashita, T. Kono, E. Nakamura, K. Otsuka, Y. Shimosaki, K. Torikai and M. Wake, Phys. Rev. Lett. 98, 054801 (2007).
- [3] K. Takayama and R. Briggs (Eds.), Chapters 11 and 12 in Induction Accelerators (Springer-Verlag, 2010) ISBN: 978-3-642-13916-1.
- [4] J. Pivarc, J. of Elect. Eng. 55, 100 (2004).
- [5] S. Gammino and G. Ciavola, Rev. Sci. Inst. 67, 155 (1996).
- [6] Atomic Data and Nuclear Data Tables 65, 1-35 (1997).
- [7] S. Gammino, G. Ciavola, L.Celona, M. Castro, F. Chines and S. Marletta, Rev. Sci. Inst. 70, 3577 (1999).
- [8] I.G. Brown, The Physics and Technology of Ion Sources (2nd Edition), John Wiley & Sons, (2004), ISBN 3-527-40410-4.